Chemical Papers (2022) 76:4203–4216
https://doi.org/10.1007/s11696-022-02111-5

ORIGINAL PAPER

Insight into the effect of alkali treatment on enhancing adsorptivity of activated carbon for HCl removal in H_2 feedstock

Anis Usmani[1,2] · Panuwat Watthaisong[3] · Nurak Grisdanurak[2] · Suwit Suthirakun[3]

Received: 13 September 2021 / Accepted: 29 January 2022 / Published online: 26 March 2022

Abstract

The removal of contaminated HCl gas in the petrochemical plants is essential to prevent corrosion problems, catalysts poisoning, and downstream contamination. Alkali-treated activated carbon (AC) was proposed as an effective adsorbent for HCl removal. Understanding the underlying mechanism of HCl adsorption on modified AC is key to design promising strategies for removal of HCl and other chlorinated hydrocarbon gases in the H_2 feedstock. Here, a combined experimental and computational approach was used to study the role of alkali treatment on the adsorption behavior of HCl on the AC surfaces. We find that an interplay between alkali ions and oxygen-containing functional groups on the AC surface plays a crucial role in stabilizing the adsorbed HCl. The origin of such stable adsorbed configurations can be attributed to the dissociative adsorption of HCl leading to a formation of low energy species such as water, OH^- and Cl^- anions. These anions are electrostatically stabilized by the alkali ions resulting in a strong adsorption of −3.61 eV and −3.69 eV for Na^+ and K^+, respectively. Close investigation on charge analysis reveals that the epoxy functional group facilitates adsorbent-surface charge transfer where O and Cl atoms gain more charges of 0.37 e and 0.58 e which is in good correlation with the improved adsorption strength. The calculated results are consistence with the experimental observations that the Langmuir adsorptivity has been enhanced upon alkali modification. The maximum adsorption capacity of AC has been improved approximately by 4 times from 78.9 to 188.9 mg/g upon treatment.

Keywords DFT · HCl removal · Graphene · Alkali treatment

Introduction

Natural gas has evolved as one of the largest and most efficient fuel for energy and electricity generation. Natural gas mainly contains methane that can be used to produce hydrogen with thermal processes such as steam-methane reformation, which therefore refers to as a H_2 feedstock (Faramawy et al. 2016). The contaminated hydrogen chloride (HCl) gas found in natural gas processing causes several problems such as pipeline corrosion, catalyst poisoning, and downstream contamination (Crum 2006). Due to its high corrosive property and ability to form various undesired chlorinated products, HCl is very much concerned and needed to be removed from the gas stream (Acelas and Flórez 2018; Wu et al. 2020).

Several strategies have been used to remove contaminated HCl from the H_2 feedstock. While the HCl gas could be eliminated by dissolving into an aqueous solution, this process accompanying large proton hydration energy is extremely exothermic where the excess heat is needed to be taken care of (Ando and Hynes 1997). Other strategies were also implemented to eliminate the HCl gas such as membrane separation, chemical reaction, and adsorption (Mouazer and Scheffer 2017; Wang et al. 2021). Gas adsorption is considered a promising approach since it is highly efficient, simple to operate, environmentally friendly, and

✉ Nurak Grisdanurak
gnurak@engr.tu.ac.th

✉ Suwit Suthirakun
suthirak@sut.ac.th

[1] Department of Chemical Engineering, Faculty of Engineering, Thammasat School of Engineering, Thammasat University, Pathumthani 12120, Thailand

[2] Center of Excellence in Environmental Catalysis and Adsorption, Thammasat University, Pathumthani 12120, Thailand

[3] School of Chemistry, Institute of Science, Suranaree University of Technology, Nakhon Ratchasima 30000, Thailand

cost effective (Benosmane et al. 2021; Liu et al. 2019; Yang et al. 2021). Several experimental studies have explored the adsorption of HCl gas onto various solid sorbents including zeolites, metal–organic framework, alkali-based sorbent, metal oxides, and activated carbon (AC) (Tolentino et al. 2020; Weinlaender et al. 2018). Among these adsorbent materials, AC has attracted much attention due to its low cost, large surface area, and various surface functional groups (Weinlaender et al. 2018).

Regarding the cited experimental works, surface oxygen atoms on the adsorbent materials could be the origin of their superior adsorptivities. In particular, an experimental study demonstrates that modification AC using NaOH solution significantly improves the adsorption capacity of the material (Cazetta et al. 2011). It was reasoned that NaOH treatment induced formation of oxygen-containing functional groups on the surface which could effectively bind to the HCl gas molecules (Wu and Tseng 2008). Nevertheless, the underlying mechanism of an interplay between alkali cations and surface oxygen atoms to facilitate the adsorption of the HCl gas has not yet been clearly explained.

Density functional theory (DFT) has been used as a tool to better understand the behavior of adsorbate on the surface in wide range of applications. For example, several computational works studied adsorption behavior of small gas molecules on AC surfaces where the local structures of AC were modeled using a graphene sheet. The calculated results reveal that these molecules only physically interact with the surface with the calculated adsorption energies in the range of 0.03–0.07 eV (Leenaerts et al. 2008; Supong et al. 2019). This is because pristine graphene exhibits well-distributed charge leading to high stability and poor reactivity. Nevertheless, it has been reported that introducing metal promoting contaminant gas resistance (Zhang et al. 2017), therefore modifying graphene structure via impurity-doping, creation of vacancies, and attaching oxygen functional groups (You et al. 2017) can significantly enhance the adsorptivity as evidenced by increasing of adsorption energy and the number of electrons transferred.

It can be seen that experiments and computations offer different merits toward the adsorption study. While experiments deliver information in accordance with macroscopic properties of sorbents and gas adsorption, absence of molecular insight forbid the fundamental understanding of the interactions. Computations, on the other hand, allow us to explore the behavior of gas adsorption at the molecular level despite their inability to provide practical macroscopic properties. In this work, we used a combined computational and experimental approach to systematically investigate the effect of alkali treatment on improving HCl adsorption on the AC surface. In particular, we carried out DFT calculations to study the interplay of the surface oxygen and alkali ions on the adsorption behavior of HCl. Pristine graphene was used as a model to represent the local structure of AC. Epoxy and hydroxyl groups and the presence of different alkali cations were considered in the model to study their effects toward HCl adsorption. Adsorption energies and electronic structures based on density of states and charge differences were analyzed to describe the character of HCl adsorption on the modified surfaces. In addition, to confirm the computational predictions, NaOH-treated AC was prepared and characterized to identify induced functional groups on the surface. HCl adsorption experiments were carried out to examine adsorption capacity of the prepared AC.

Materials and method

Computational details

All calculations were carried out using the spin polarized density functional theory (Kohn and Sham 1965) with periodic boundary conditions as implemented in the Vienna ab initio simulation package (VASP 5.3) (Kresse and Furthmuller 1996; Kresse and Furthmüller 1996; Kresse and Hafner 1993). The Perdew–Burke–Ernzerhof form of generalized gradient approximation was chosen as the exchange–correlation functional (Perdew et al. 1996). We used the Grimme's correction method (DFT-D3) to properly take into account the van der Waals interaction between surface and adsorbates (Grimme et al. 2011). The projector augmented-wave method (Blöchl 1994; Kresse and Joubert 1999) was employed to describe nucleus and core electron potentials where their valence-electron wave functions were expanded in plane-wave basis with a cutoff energy of 400 eV. The treated valence electrons are O $2s2p$, C $2s2p$, H 1 s, and Na $2p3s$. The convergence criteria of the self-consistent field are within 1.0×10^{-6} eV whereas the force convergence of ionic relaxation was set to 0.02 eV/Å.

We constructed a 5×5 supercell of pristine graphene (p-graphene) containing 50 carbon atoms to model the local structure of AC surfaces. A 15 Å vacuum gap was added in the normal direction to avoid spurious interactions between periodic images. Various foreign atoms were added on the graphene to simulate the modified AC surfaces including epoxy group, hydroxyl group, and alkali metal atoms (Na and K). Behavior of HCl adsorption was explored at different conditions of pristine and modified graphene where their internal coordinates were relaxed using a $4\times4\times1$ Γ-centered k-point grid. The adsorption energies, E_{ads}, were then calculated using Eq. (1).

$$E_{ads} = E_{HCL/surface} - \left(E_{surface} + E_{HCL}\right) \quad (1)$$

where $E_{HCl/surface}$, $E_{surface}$, and E_{HCl} represent the total energies of systems containing adsorbed HCl on the surface, the surface, and the gas-phase HCl molecule, respectively.

The electronic structures of the adsorbate and graphene systems were investigated by analyzing their Bader charges (Henkelman et al. 2006; Sanville et al. 2007) and projected density of states (PDOS). To closely investigate the origin of the improved adsorption strength between the HCl gas and surface species, Bader charge analysis implemented by Sanville et al. (2007) was performed where the charge distribution before and after adsorption was analyzed. Charges on atoms were determined by assigning an integration number of electronic charge density where Bader uses zero-flux surfaces to define the integration region of each atom. The bonding character of the newly formed compounds can be better understood by analyzing their projected density of states (PDOS). PDOS calculations reveal the contribution of atomic orbitals toward electronic structure of the surface where number of different states at a particular energy level are projected to an atom type (Menezes and Ullah 2021).

In addition, thermodynamic properties of an isolated HCl gas molecule were calculated using the quantum chemical program TURBOMOLE version 7.2 (Ahlrichs et al. 1989; GmbH 2010). Optimization of the molecular geometries and frequency calculations has been carried out at the B3LYP/TZVP (Becke 1993; Schäfer et al. 1994) level of theory. Thermodynamic properties were calculated under different temperatures and a constant pressure of 1 atm.

In order to fully investigate the thermodynamic stability of adsorbed HCl molecules on AC and modified AC, we carried out constrained ab initio thermodynamic calculations to account for the effects of temperatures and HCl partial pressure at operating conditions. The Gibbs free energies of adsorption, G_{ads}, were computed using Eq. (2)

$$G_{\text{ads}} = E_{\text{ads}} + \Delta\text{ZPE} - k_B T \ln \frac{Q_{\text{surface/HCl}}}{Q_{\text{surface/HCl}} Q_{\text{HCl}}} - k_B T \ln \frac{P_{\text{HCl}}}{P^0} \quad (2)$$

where ΔZPE is the difference of zero-point energy $\left(\text{ZPE} = \sum_{j=1}^{N_i} \frac{h\nu_j}{2}\right)$ between the product state (adsorbed molecule on the surface) and the reactant states (gas-phase HCl and bare surface) with ν_j being the vibrational frequency of the jth mode and N_i being the number of vibrational modes. The partition functions of the adsorbed HCl on the surface, $Q_{\text{surface/HCl}}$, and the surface prior adsorption, Q_{surface}, were calculated using only the vibrational contributions whereas that of the gas-phase molecule, Q_{HCl}, took into consideration all contributions from rotational, translational, and vibrational partition functions. The effect of HCl partial pressure on the Gibbs free energy of adsorption is obtained assuming the gas phase is ideal as corrected via the $k_B T \ln \frac{P_{HCl}}{P^0}$ term. Negative G_{ads} indicates thermodynamically stable adsorption of HCl at the considered temperature and pressure.

Experiments

Preparation of NaOH-treated activated carbon

The activated carbon (AC) derived from coconut shell was obtained [Puresorb co. Ltd., Thailand]. Chemicals and gases including sodium hydroxide (NaOH) pellets [Merck Co., Ltd, Germany], 99.99% purity of hydrogen gas [TIG Co. Ltd., Thailand], 600 ppm of hydrogen chloride (HCl) [TIG Co. Ltd., Thailand] were used. The NaOH-treated AC was prepared by an impregnation technique. The 12 g of AC in granular form with 0.5 g/L bulk density was soaked in a 6 and 12 mol/L NaOH solution for 4 h. The treated AC was consequently filtered and dried at 80 °C for overnight. Then, 0.1 g of the treated AC was placed onto a plastic plate inside an enclosed plastic adsorption chamber.

Characterization

Both prior and spent adsorbents were characterized for physical and chemical properties. The surface functional groups were characterized using the Fourier transforms infrared (FTIR) spectroscopy (Vertex 80/80 V, Bruker, Germany). X-ray diffraction (XRD) patterns were gathered from diffractometer (Bruker D8 advanced, Germany) equipped with Cu Kα radiation source at 40 kV. The surface area was characterized by N_2 sorption using Brunauer–Emmett–Teller (BET) technique (Autosorb-1, chrantachrome, BL model). Scanning electron microscope (SEM) equipped with electron-dispersive X-ray spectroscopy (EDS) were used for surface morphology characterization and environmental analysis (JEOL Electron Microscope, model JSM-5410LV and EDS Oxford Energy-Dispersive X-ray spectrometer model INCA-350).

HCl adsorption test

The adsorption experiments were carried at constant temperature of 35 °C. Prior to each adsorption test, the chamber was filled with N_2 followed by vacuuming until the pressure inside the chamber was below 1 torr. The initial 600 ppm of hydrogen chloride (HCl) was used at initial. The 50 ml/min of feed gas was initially mixed in a chamber by 30 mL/min of HCl balanced in H_2 and 20 ml/min of H_2 (99.99%). The feed gas was kept for 45 min until the final HCl concentration was 500 ppm. Concentrations remaining in the chamber

were measured using a gas detector tube with a detection limit of 0.05 ppm.

To examine the lifespan of the adsorbent, we carried out the gaseous breakthrough experiments that used to describe the deactivation time of the adsorbent where the gas molecules are unable to adsorb on the surface. The breakthrough curves defined as a plot of period of the test versus the concentration of the adsorbate in the outlet stream (Marsh and Rodríguez-Reinoso 2006). The experiments were carried out with packed column where the adsorbents were packed inside the reactor. The integrated area under the curve represents the HCl gas transfer to adsorbents which determines the adsorbent lifespan. The breakthrough can be calculated by Eq. (3).

$$\tau = \int_0^\infty \left(1 - \frac{C}{C_0}\right) \mathrm{d}t \tag{3}$$

where C and C_0 represents the HCl concentration at the effluent and influent, respectively.

Results and discussion

HCl adsorption on *p*-graphene and epoxy graphene

To obtain insight into the adsorption behavior of HCl on various AC surfaces, we employed a first-principles method based on DFT to explore its adsorption modes and calculate their adsorption energies. According to the experimental observations, typical AC comprises 88% C, 6–7% O, 0.5% H, 0.5% N, and 1% S where the variation of O contents depend on the treatment process and the types of raw material to produce the AC (Ludlow 2006). It can be seen that majority of the AC structure is mostly three—coordinated carbon with decorated oxygen atoms as also reported in previous studies (Boehm 1966; Boehm et al. 1964). Several oxygen functional groups were experimentally observed on the AC surfaces such as epoxy, ketones, alcohols, and carboxylic acids at high coverage (Donnet 1968). However, a high coverage of oxygenated groups would make the system more complex whereas less complicated low coverage model can effectively be used to obtain insight into the role of oxygenated functional group toward the HCl adsorption. Among these oxygenated functional groups, the epoxy group has been predicted by Ab initio molecular dynamic simulations (AIMD) as one of the most stable functional groups in the reduced graphene oxide system. Experimental results show that these oxygenated functional groups are quite persistent even under aggressive chemical and thermal treatment (Bagri et al. 2010). Hence, in this work, a bare graphene and epoxy graphene sheets were as a model system to study behavior of HCl adsorption.

Several adsorption modes of HCl were examined to find the most stable adsorbed configurations. Computations show that HCl molecularly adsorbs on the *p*-graphene surface. Two adsorption modes were considered in this study including perpendicular adsorption of HCl with H (H-end mode) and Cl (Cl^- end mode) pointed to the surface, as shown in Fig. 1. It can be seen that the most stable configurations are the H-end configurations which are more stable than those of the H-end mode by 0.15 eV and 0.32 eV for adsorption on *p*-and epoxy graphene, respectively (Fig. 1). The structure of the adsorb molecule also agrees with the calculated adsorption energies where the more stable H-end mode exhibits closer molecule-surface distances for p-graphene (218 vs. 312 pm) and epoxy graphene (174 vs. 302 pm).

Next, the effect of an epoxy functional group on the adsorptivity was closely investigated. As shown in Fig. 2a, for the adsorption on p-graphene, the most stable configuration exhibits a perpendicular orientation of the HCl molecule with the H atom closest to the surface. The calculated

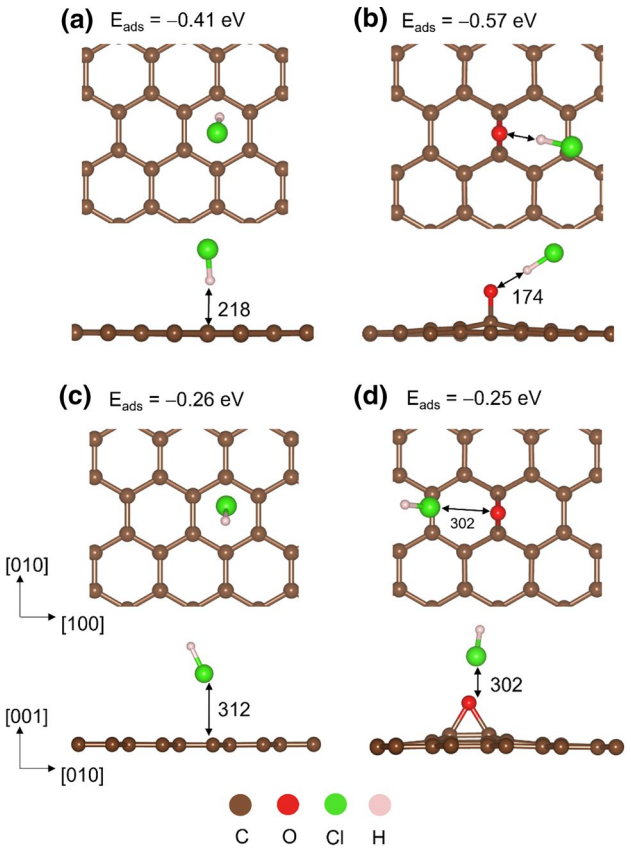

Fig. 1 The HCl adsorption modes including **a** H^- end mode for pristine graphene, **b** H^- end mode for epoxy functional group, **c** Cl^- end mode for pristine graphene, and **d** Cl^- end mode for epoxy functional group

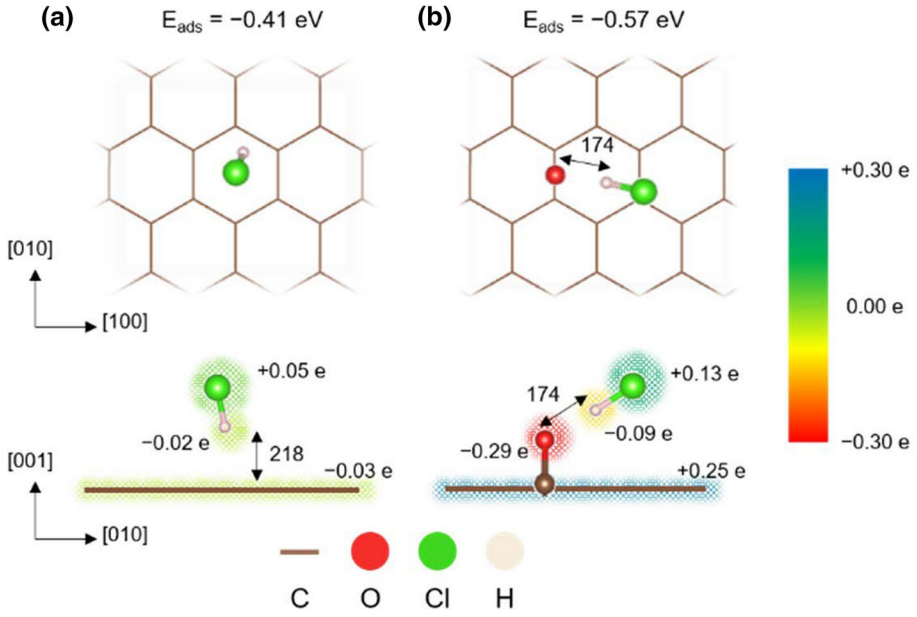

Fig. 2 Schematic illustrations of most stable configurations, equilibrium distances, degree of charge transferred, and adsorption energies of HCl on **a** pristine graphene and **b** epoxy graphene. The equilibrium distances are denoted in pm. The shadow colors indicate the extent of charge transferred upon adsorption

adsorption energy of −0.41 eV indicates that the HCl molecule physically adsorbs on the *p*-graphene where the distance between the molecule and the surface is 218 pm. The most stable adsorption mode is equivalent to that of reported in a recently published work where our calculated adsorption energy is somewhat stronger than their reported value of −0.23 eV. The mismatched adsorption energies may stem from the lack of weak vdW corrections in their computational treatment (Ran et al. 2020).

In the presence of the epoxy group, HCl adsorbs more strongly on the surface where its adsorption energy is improved from −0.41 to −0.57 eV; nevertheless, it is still considered as weak physisorption, Fig. 2b. The adsorption mode is quite similar to that of the *p*-graphene where HCl is molecularly adsorbed on the surface. Its H atom points toward the epoxy group forming a weak H-bond interaction with the O–H distance of 1.74 Å, Fig. 2b. The stronger interaction between the HCl molecule and the epoxy group leads to an elongation of H–Cl bond distance by 2 pm when compare with that of the adsorbed molecule on the bare surface.

To obtain insight into the role of epoxy group in the improved adsorption, we analyzed their charges using the Bader charge scheme (Yu and Trinkle 2011). For adsorption on the *p*-graphene, the charge of 0.03 e is transferred from the surface to the HCl molecule where it is mostly accumulated at the more electronegative atom, Cl, as shown in Fig. 2a. The degree of charge transfer is slightly greater when an epoxy group was introduced onto the surface where 0.04 e is transferred from the epoxy graphene to the HCl molecule, Fig. 2b. It is obvious that the epoxy oxygen acts as the adsorbed center where the charge of the oxygen atom is depleted by 0.29 e. The analysis suggests that the presence of the epoxy group facilitates adsorbent-surface charge transfer, which improves adsorptivity of the AC surface. It can be concluded that the epoxy group serves as a charge transfer center which stabilize the HCl adsorption.

In addition, we calculated and analyzed the projected density of states (PDOS) of the adsorbed HCl and compare

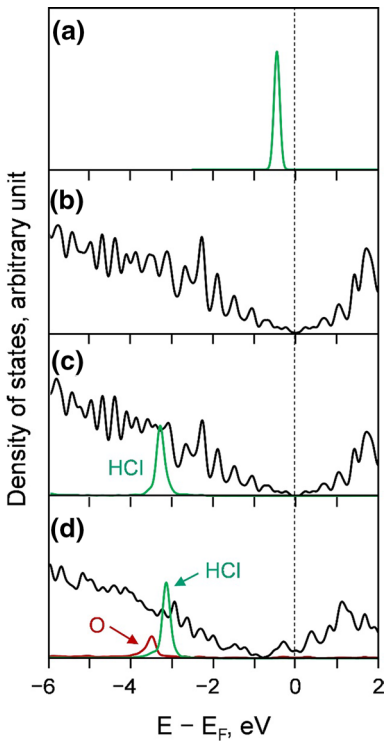

Fig. 3 Projected density of states of **a** HCl gas, **b** pristine graphene, **c** HCl adsorbed pristine graphene, and **d** HCl adsorbed epoxy graphene. The vertical dashed line marks the Fermi energy

with that of the HCl gas molecule to gain deeper understanding on the interaction between HCl and the graphene surface. The DOS of a single HCl molecule exhibits sharp frontier states at the Fermi level, as shown in Fig. 3a. When the molecule is adsorbed on the p-graphene, these states become more diffuse and shift to the lower energy, Fig. 3c. This indicates that HCl prefers to adsorb on the graphene surface which is consistent with the calculated adsorption energy. When HCl adorbs at the epoxy site, the states of HCl molecule largely hybridize with the O 2p states suggesting strong interaction between HCl and the O functional group on the surface, Fig. 3d. The calculated DOS explains the improved adsorption energy and higher degree of charge transfer in the presence of epoxy group.

From the computational viewpoints, it can be concluded that oxygen-containing functional groups occurred upon base treatment improve the adsorption strength of the HCl molecule. Analysis of electronic structures reveals that O on the surface act as active sites for HCl adsorption. Although the presence of oxygen functional groups enhances the adsorption, these interactions are still characterized as weak van der Waals force where HCl molecules only physisorbed on the surface without formation of chemical bonds.

Interplay between alkali cations and surface oxygen functional groups

Upon the alkali treatment, it is likely that not only oxygen functional groups are introduced but also large amounts of alkali ions could co-exist on the surface. Hence, to study the role of alkali cations on the adsorptivity, the graphene model was modified by adding various co-adsorbed O atom and alkali ion (M = Na, K) on the surface. The following co-adsorbed functional groups were considered; hydroxyl with an alkali ion (MOH) and epoxy with two alkali ions (M_2O) where the considered alkali ions are Na^+ and K^+ cations. The calculations were performed by initially optimizing the MOH and M_2O surfaces and an isolated HCl molecule. Then, the HCl molecule was placed nearby the OH of O functional group and the metal cation where H of the HCl molecule is closer to the OH/O group and Cl is next to the metal ion. Next, the geometry optimizations were carried out to yield to optimized structures. The most stable configurations where selected where their energies were used to calculated E_{ads}.

In the case of the MOH graphene, we find that the HCl molecule dissociatively adsorbs on the surface. This process is barrierless with the adsorption energies of −2.76 eV and −2.73 eV for M = Na^+ and K^+ ions, respectively. As shown in Fig. 4a, the H atom forms a covalent bond with the surface hydroxyl group and yield a water molecule with asymmetric O–H bond distances of 100 and 97 pm for both Na^+ and K^+ containing surfaces. The Cl^- anion electrostatically attracted to the nearby alkali cation at the distances of 252 pm and 282 pm for Na^+ and K^+ ions, respectively. The farther distance between Cl and K is due to the larger ionic radius of K^+ ion (138 pm) than that of the Na^+ ion (102 pm) (Shannon 1976). The newly formed water molecule is intact with the M–Cl dimer where the distances between the O atom and the alkali ions are 228 and 261 pm for Na^+ and K^+ ions, respectively. Such strong interactions lead to highly stabilized adsorbates on the graphene as reflected by dramatically decreased adsorption energies.

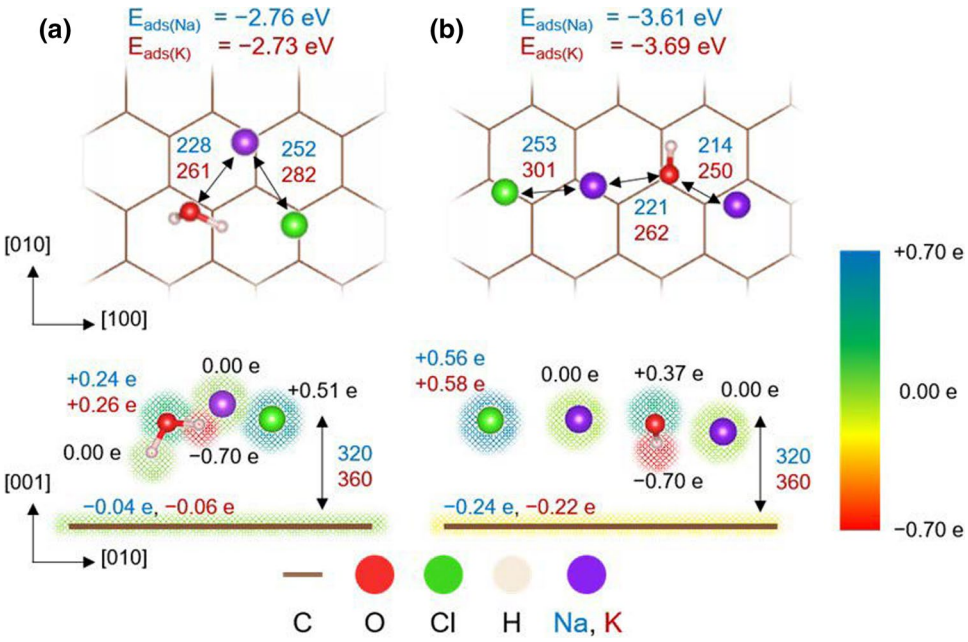

Fig. 4 Schematic illustrations of most stable configurations, equilibrium distances, degree of charge transferred, and adsorption energies of HCl on **a** MOH graphene and **b** M_2O graphene (M = Na, K). The equilibrium distances are denoted in pm. The shadow colors indicate the extent of charge transferred upon adsorption where the positive and negative values indicate charge gain and charge loss, respectively

Even more stable co-adsorbed species were predicted for HCl adsorption on the M_2O graphene where the adsorption energies are −3.61 eV and −3.69 eV for Na^+ and K^+ ions, respectively. Similar to the previous case, the adsorbed HCl molecule dissociates where the H atom forms a new bond with the surface O atom and yields a hydroxyl group with an O–H bond distance of 97 pm, Fig. 4b. The Cl^- anion then attracted to the nearby alkali ion with the distances of 253 pm and 301 pm for Na^+ and K^+ ions, respectively. The generated OH group is relatively close to the two alkali ions with the average M–O distances of 218 pm and 256 pm for Na^+ and K^+ ions, respectively. Such stable co-adsorbed species could be attributed by the presence of two anion species, Cl^- and OH^-, which electrostatically interact with two alkali ions on the surface.

Although the calculated adsorption energies of HCl on the alkali-modified surfaces are extremely low, the binding energies between the newly formed adsorbed species and the surface are rather moderate. The calculated binding energies are in the range of 0.78–1.07 eV which imply that these adsorbed species could easily be separated from the surface. As a result, from the computational viewpoint, the post-adsorbed AC could be treated to easily remove the adsorbed species and regenerate the fresh adsorbent. As confirmed by the experimental results, NaCl has been deposited on the spent adsorbent (discussed in Sect. 4) which is easily washed by water and consequently dry before reuse.

The Bader charge analysis reveals significantly greater charge transfer upon HCl adsorption on the alkali-modified graphene as compared to that of the p-graphene. As depicted in Fig. 4a, the MOH graphene involves charge transfer of 0.19 e from the HCl to the M-OH species and the graphene sheet. In particular, the H atom of HCl mostly loses its charge (−0.70 e) to the surface oxygen atom (+0.24 e and +0.26 e for Na and K systems) and Cl atom (+0.51 e); thus, it is considered as H^+ when it bonds with the OH^- ion and yields a H_2O molecule. As the Cl atom accepts charge of 0.51 e, it can be considered as a Cl^- anion which electrostatically attracted to the remaining alkali cation where their charges remain unchanged (0.00 e). Likewise, the behavior of charge transfer for the M_2O graphene is similar to those of the MOH graphene. Nevertheless, the degree of charge transfer is greater for the M_2O graphene where O and Cl atoms gain more charges of 0.37 e and 0.58 e, respectively. As a result, more stable adsorbed species were obtained where the adsorption energies have been lowered to –3.61 and −3.69 eV for surfaces containing Na^+ and K^+ ions, respectively.

As previously discussed, the HCl molecule undergoes dissociative adsorption on the alkali-modified surfaces and form new compounds, i.e., water and chloride salts. It can be seen from Fig. 5a, b that the PDOS of the H_2O molecule is located at low energy levels and the Cl states shift further

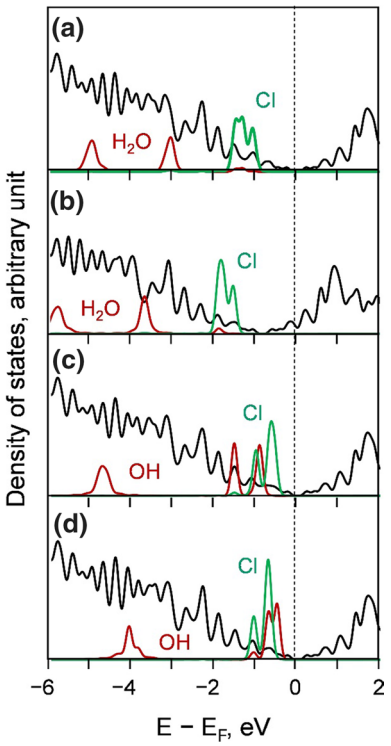

Fig. 5 Projected density of states of HCl adsorption on graphene as modified by **a** NaOH, **b** KOH, **c** Na_2O, and **d** K_2O. The vertical dashed line marks the Fermi energy

below the Fermi level. These shifts indicate that formations of the H_2O molecule and Cl^- anion are quite stable on the surface. In addition, the PDOS of HCl adsorbed on the M_2O graphene reveal the strongly hybridized OH^- and Cl^- states (Fig. 5c, d). Such strong hybridization implies that the newly formed OH^- and Cl^- species are both stabilized by the electrostatic interactions with the two alkali cations on the surface, which in turn, leads to the very stable adsorbed species. Nevertheless, the PDOS of newly formed adsorbed species, i.e., M–Cl, OH, and H_2O, moderately overlap with that of the graphene sheet implying weak interactions between these species and the adsorbent. The calculated PDOS are in good agreement with the discussion of the Bader charge analysis and adsorption energies which imply strong interaction between the co-adsorbed species.

Thermodynamic stabilities of HCl adsorption

At the operating temperature of 35 °C, the calculated G_{ads} decreases with increasing partial pressure of HCl suggesting that adsorption capacity of the surface is greater at high HCl concentration, Fig. 6a. Among the considered AC surfaces, the alkali-modified surfaces affectively adsorb HCl as their calculated G_{ads} are negative at all considered HCl concentration. On the other hand, the untreated AC, as modeled by

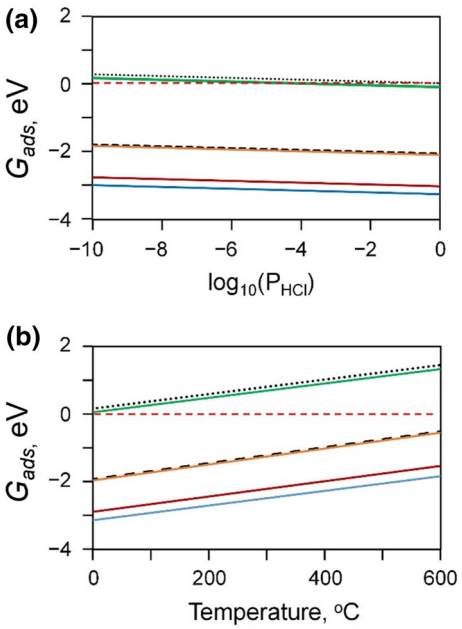

Fig. 6 Calculated Gibbs free energies of adsorption, G_{ads}, as a function of **a** partial pressure of HCl gas at 35 °C and **b** operating temperature of 35 °C at constant HCl concentration of 600 ppm. The dotted black, green, orange, dashed black, red, and blue lines denote the G_{ads} of pristine, epoxy, NaOH, KOH, Na_2O, and K_2O graphene, respectively. The dashed red line marks the G_{ads} of zero eV

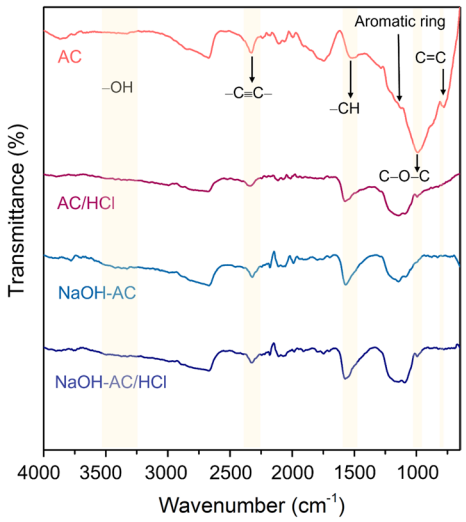

Fig. 7 Schematic illustration of Fourier-transform infrared spectroscopy, FTIR, spectra of untreated-(AC), post-adsorbed activated carbon (AC /HCl), $NaOH^-$ treated-(AC-NaOH), and post-adsorbed $NaOH^-$ treated activated carbon (AC-NaOH/HCl)

pristine and epoxy graphene, display positive G_{ads} at most range of considered HCl concentrations indicating low adsorptivity toward HCl gas. Only the epoxy surface starts to adsorb at relatively high HCl pressure of 0.1 atm.

Effect of temperature on the adsorptivity was explored where the G_{ads} were calculated as a function of temperature at constant HCl concentration of 400 ppm as used in the experiment. It can be seen from Fig. 6b that increasing the temperature leads to increasing G_{ads} indicating lower adsorptivity. Such behavior is expected because increasing temperature lowers chemical potential of HCl gas resulting in relatively low adsorption capacity (Iannarelli and Rossi 2014; Weinlaender et al. 2018). Here, again, only the alkali-modified surfaces act as effective adsorbate whereas the untreated AC does not adsorb HCl gas at the considered temperature range, even at low temperature of 0 °C. Overall, it can be concluded that at operating conditions, the untreated AC is inert toward HCl adsorption. The adsorptivity can be greatly improved via alkali treatment where the calculated adsorption free energies are negative at wide range of temperatures and HCl concentrations.

Characterizations and HCl adsorption tests

To confirm the computational predictions on the superior adsorptivity of the alkali-modified AC, various characterizations of the adsorbents and adsorption experiments were carried out. First, the functional groups of the adsorbents were characterized using the FTIR technique. It can be seen from Fig. 7a that the untreated AC mainly comprises aromatic carbon rings indicated as broad peak at 1130 cm^{-1} (Chen et al. 2014). For the NaOH-modified AC, the aromaticity was largely destroyed by the alkali treatment where the peak at 1130 cm^{-1} is greatly diminished. On the other hand, the band of O–H stretching at 3542 cm^{-1} was observed in the IR spectra of the alkali-treated samples (Protilla 1976). The carbonaceous structures were deconstructed after HCl adsorption and surface modifications as resulted from the decreases of C = C and C≡C bonds spectra at 776 and 2327 cm^{-1}. Importantly, an increase in the band at 1000–1300 cm^{-1} attributed to C–O– C single bonds (Kim et al. 2006) was also found in prior and post-adsorption of alkali-treated samples. This implies that parts of the AC surface were restructured via modification of oxygenated functional groups and deposition of alkali metal (Hu and Hsieh 2017; Tangsathitkulchai et al. 2021). The–CH bond spectrum is sharper and higher intensity after NaOH modification and adsorption. Carbon might lose the stability. The H of HCl thus could physically or chemically attach the surface carbon.

With an enhancement of surface via base treatment, the Brunauer–Emmett–Teller (BET) and scanning electron microscopy equipped energy-dispersive X-ray (SEM–EDX) characterizations were carried out to identify the effects of NaOH treatment on the AC surfaces. The BET analysis reveals that base treatment decreases the surface area of the adsorbent by 1.38 times, from 1010 ± 27 to 732 ± 51

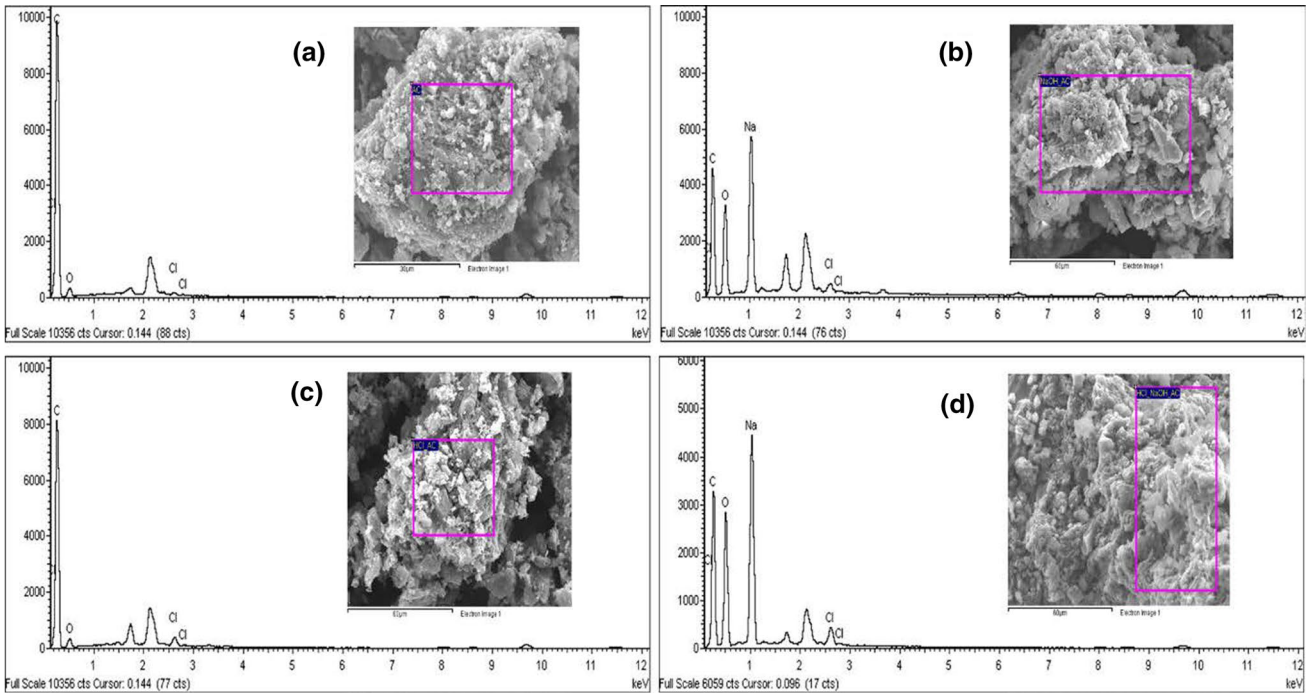

Fig. 8 Schematic illustrations of SEM–EDX of **a** AC, **b** NaOH-treated AC, **c** HCl adsorbed AC, and **d** HCl adsorbed $NaOH^-$ treated AC

Table 1 Results of the elemental analysis by SEM − EDX

Elements	Weight (%)			
	AC	HCl/AC	NaOH-AC	HCl/NaOH–AC
C K	86.64	85.61	47.04	44.78
O K	12.90	13.55	36.07	36.17
Cl K	0.47	0.84	0.76	1.68
Na K	NA	NA	16.13	16.37

NA = Not available

m^3/g. This is due to the accumulation of alkali metal on the surface. The existence of Na metal was confirmed by the SEM–EDX analysis as shown in Fig. 8 and summarized in Table 1. It can be seen that significant amounts of Na present on the treated AC (16.13%). In addition, the NaOH-treated AC surface exhibits small cavities as compared with that of the untreated AC where the flake-like particles show the deposition of Na on the AC surface, as shown in Fig. 9.

After HCl adsorption, the Na metal is still intact with comparable Na content to that of AC prior adsorption (16.13 vs. 16.37%), as detailed in Table 1. The Cl uptake by the prepared adsorbent is confirmed by the EDX analysis. The increasing of Cl content after HCl adsorption for the treated AC (1.68–0.76 = 0.92%) is greater than that of the untreated AC (0.84–0.47 = 0.37%). This indicates that NaOH treatment improves HCl adsorption capacity. The experimental observations agree very well with the calculated results that the NaOH-modified AC systems exhibit stronger HCl adsorptivity.

In addition, the addition of alkali solution subjected to increase surface polarity such as acidic and basic functional group on surface (Boehm 1966). The XRD pattern reported the unchanged crystalline structure after NaOH treatment as also reported previously (Wang et al. 2020). Na^+ ion remains on the adsorbate which consequently polarized inducing the Cl^- ion and forming NaCl as the crystalline phase.

After HCl adsorption, the NaOH-modified AC was characterized using the XRD technique to confirm the formation of ionic metal chloride compounds as predicted in the DFT calculations. As shown in Fig. 10, the spent NaOH-treated AC exhibits characteristic patterns of NaCl crystal with low intensity of characteristic carbon peak around two-theta of 25 degree representing with oxide. The presence of NaCl was previously reported for Na-treated adsorbent in chloride ion treatment (Osio-Norgaard and Srubar 2019). The experimental results are consistent with the computational predictions that HCl dissociatively adsorbs on the alkali-modified AC. The Cl^- ions electrostatically attract to the Na + ions leading to a formation of NaCl compound (Artemov et al. 2015).

Lastly, the adsorptivity of the AC and NaOH-modified AC toward HCl gas was determined using the Langmuir isotherm model as calculated using Eq. (4) (Swenson and Stadie 2019).

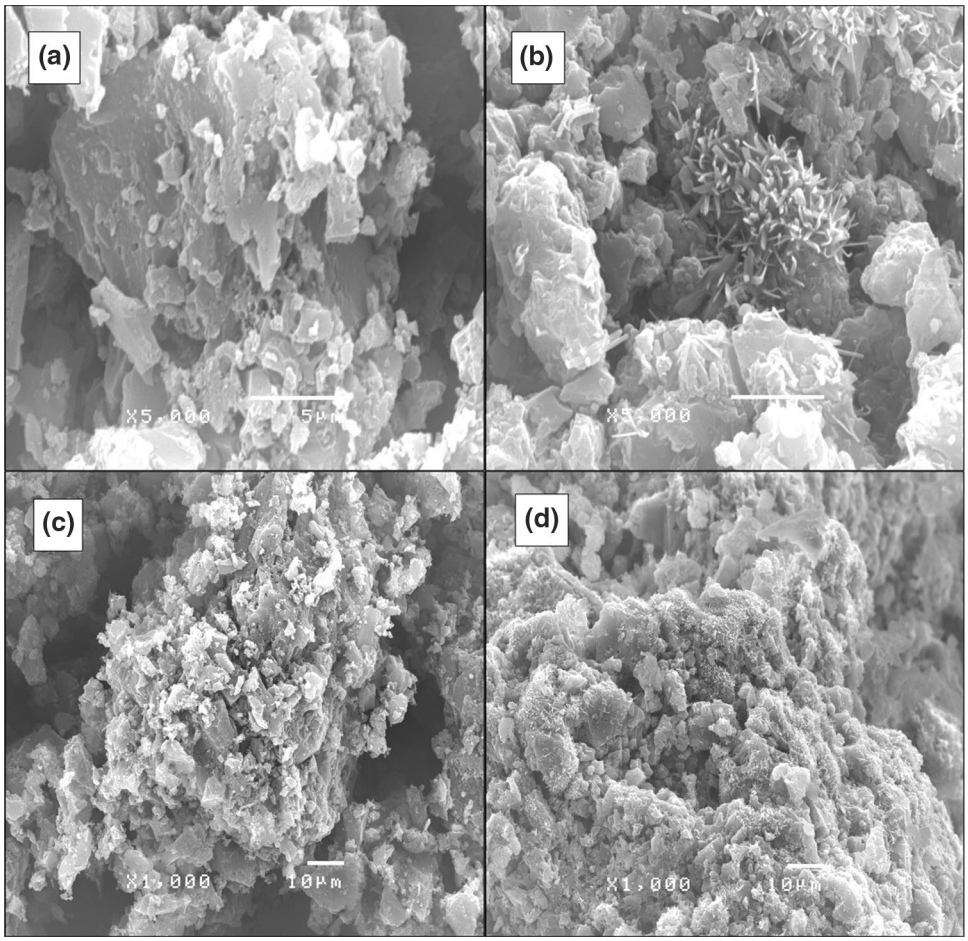

Fig. 9 Micrograph of prior and after adsorption with 5,000 magnification of **a** AC and **b** $NaOH^-$ treated AC and 1000 magnification of **c** HCl adsorbed AC and **d** HCl adsorbed $NaOH^-$ treated AC

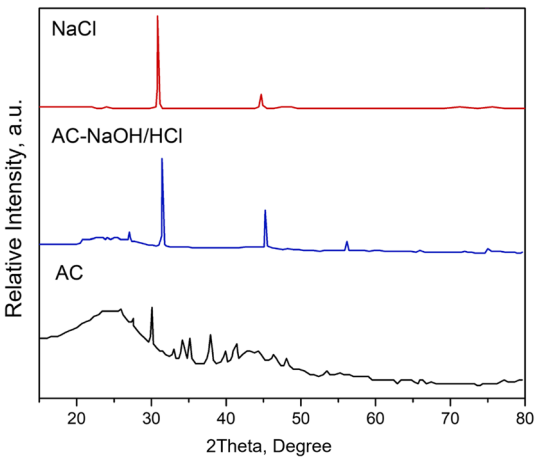

Fig. 10 Schematic illustration of X-ray diffraction, XRD, patterns of untreated-(AC), $NaOH^-$ treated-(AC-NaOH), and post-adsorbed $NaOH^-$ treated activated carbon (AC-NaOH/HCl) adsorption on NaOH-treated AC

$$q_e = \frac{(q_m \times K_L \times C_e)}{[1 + (K_L \times C_e)]} \tag{4}$$

where q_e and q_m represent the equilibrium and maximum loading capacity, respectively; C_e refers to the equilibrium HCl concentration in gas phase; and K_L is the Langmuir equilibrium constant which related to the affinity of binding sites with the adsorbate, where the linearized term is as Eq. (5).

$$\frac{C_e}{q_e} = \frac{1}{q_m K_L} + \frac{C_e}{q_m} \tag{5}$$

As shown in Fig. 9, the HCl adsorption on both adsorbents exhibits well−fitted by Langmuir model ($R^2 = 0.9737$ and 0.9897) indicating that monolayer of adsorbed molecules takes place over both surfaces, Fig. 11. It is characterized by the plateau that no further adsorption takes place on both surfaces. As summarized in Table 2, the calculated maximum adsorption capacity, q_m, for the modified AC surface (188.9 mg/g) is substantially higher than that of the untreated AC surface (78.9 mg/g). The estimated adsorption capacity is also consistent with the adsorption coefficient,

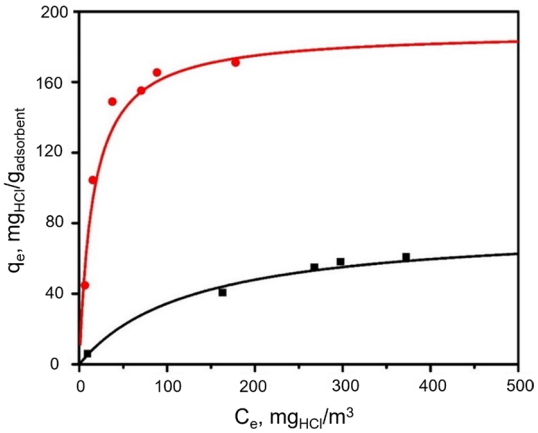

Fig. 11 Langmuir adsorption isotherm fitting of HCl adsorption on untreated AC (black filled square) and $NaOH^-$ treated AC (black filled circle)

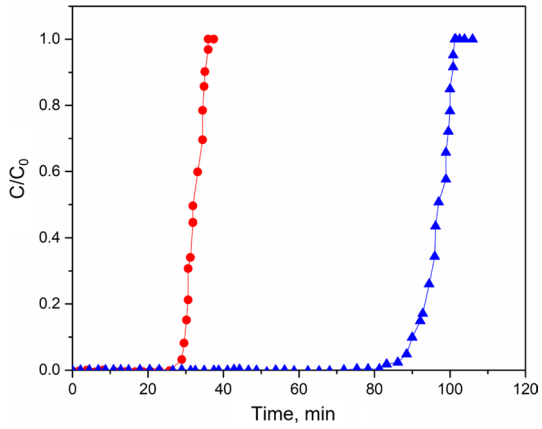

Fig. 12 The breakthrough curves of HCl adsorption in packed bed column at 35 °C on AC (black filled circle) and NaOH-treated AC (black filled triangle)

Table 2 Langmuir isotherm parameters

Adsorbent	q_m ($mg_{HCl}/g_{adsorbent}$)	K_L ($g_{adsorbent}/m^3$)	R^2
AC	78.74	0.00779	0.9867
NaOH-treated AC	188.68	0.06393	0.9940

K_L, that the modified AC displays a significantly higher value of 0.064 $g_{adsorbent}/m^3$ whereas the unmodified AC possesses a much smaller adsorption coefficient of 0.008 $g_{adsorbent}/m^3$. The identical relationship was observed in previous study (Yue et al. 2006) where the adsorption capacity of CO_2 and H_2 is higher using NaOH-modified activated carbon and the higher dichlorination amount using modified activated carbon (Chen et al. 2014). Langmuir isotherm suggests that there is one monolayer of HCl physically adsorbed on the AC where the adsorbates homogeneously cover the adsorbent surface (Swenson and Stadie 2019). The experimental results illustrate the adsorption of Langmuir isotherm which imply that interaction between adsorbate and adsorbent is significant corresponding to the computational results. The results obtained from adsorption isotherm are consistent with the DFT-calculated results that the alkali treatment improves adsorptivity of the AC adsorbents.

As a conclusion, surface modification via NaOH could lower surface area and improve surface basicity that facilitate the gas removal (Soni et al. 2020). The coconut shell-based AC as used in the study basically has large amounts of basic sites (Lee et al. 2010). The basicity on AC was attributed to the formation of oxygenated function groups (hydroxyl and epoxy) which help stabilize HCl adsorption. With the cracked surface and alkali deposition, the enhancement through surface modification is obviously resulted in increasing adsorption capacity of HCl.

Breakthrough curves of HCl adsorption

It can be seen from Fig. 12 that the NaOH-treated AC exhibits significantly longer lifespan (3.2 times) than that of the untreated AC. The experimental results are consistent with the calculated adsorption energies that the NaOH-treated AC shows a superior adsorptivity. Once breakthrough occurs, the adsorbent must be regenerated or disposed. In practice, the adsorbent is generally used to adsorb various contaminated substances in the natural gas stream including gaseous HCl, chlorinated compounds, and various heavy metal elements. The regeneration process involves the removal of strongly adsorbed heavy metals which is rather complicated. Therefore, the regeneration of exhausted adsorbent is generally not carried out and is transferred to disposal (Georgiadis et al. 2020). Nevertheless, the regeneration of such adsorbents, where removal of heavy metals is crucial, is of particular interest and could be our future study.

Conclusion

We used the combined experimental and computational approaches to explore the role of alkali treatment toward the HCl gas adsorption on AC. Characterization based on FTIR and XRD shows that upon the NaOH treatment, higher concentration of oxygen-containing functional groups and significant amounts of Na^+ ions are expected on the modified AC surfaces. The BET analysis reveals that base treatment decreases the surface area of the adsorbent by 1.38 times with the Cl uptake increased by 0.55%. It is obviously shown through the adsorption experiments that the alkali treatment has dramatically improved the adsorptivity of the AC approximately 2.4 times within the description of Langmuir isotherm. Computations based on first-principles

method reveal the underlying mechanism of the role of alkali treatment on enhancing the adsorption performance of the AC. Oxygen functional groups on the surface as modeled by an epoxy group help to stabilize the adsorbed HCl; however, the improved adsorption energy is rather small. The drastic improvement in adsorptivity is predicted when alkali ions such as Na^+ and K^+ are incorporated on the surface where their adsorption energies have been improved by six to seven folds. Illustrated through their electronic structures, the alkali ions act as positive counter ions to electrostatically stabilize the co-adsorbed Cl^- ions and, therefore, promotes dissociative HCl adsorption. The calculated results are consistence with the XRD characterization revealing the existence of NaCl phase on the AC after HCl adsorption. In addition, the thermodynamics model was employed to predict the relative stabilities of adsorbed HCl at various temperatures and HCl concentrations. Computations show that only the alkali-modified AC can significantly adsorb the HCl gas at the operating conditions. The insight obtained based on the microscopic investigation can explain the experimentally observations of the improved adsorptivity of the alkali-treated AC surfaces.

Funding This work was funded by Suranaree University of Technology (Research Grant No. 16/2563). We would like to thank Institute of Science, Suranaree University of Technology; the Synchrotron Light Research Institute (SLRI); and National e-Science Infrastructure Consortium, Thailand, for computational resources.

Data availability The data that support the findings of this study are available from the corresponding author upon reasonable request.

Declarations

Conflict of interest On behalf of all authors, the corresponding author states that there is no conflict of interest**.**

References

Acelas NY, Flórez E (2018) Chloride adsorption on Fe- and Al-(hydr) oxide: estimation of gibbs free energies. Adsorption 24:243–248. https://doi.org/10.1007/s10450-018-9939-0

Ahlrichs R, Bär M, Häser M, Horn H, Kölmel C (1989) Electronic structure calculations on workstation computers: the program system turbomole. Chem Phys Lett 162:165. https://doi.org/10.1016/0009-2614(89)85118-8

Ando K, Hynes JT (1997) Molecular mechanism of HCl acid ionization in water: ab initio potential energy surfaces and monte carlo simulations. J Phys Chem B 101:10464–10478. https://doi.org/10.1021/jp970173j

Artemov V, Volkov A, Sysoev N (2015) Conductivity of aqueous HCl, NaOH and NaCl solutions: is water just a substrate? EPL 109:10464–10478. https://doi.org/10.1209/0295-5075/109/26002

Bagri A, Mattevi C, Acik M, Chabal YJ, Chhowalla M, Shenoy VB (2010) Structural evolution during the reduction of chemically derived graphene oxide. Nat Chem 2:581–587. https://doi.org/10.1038/nchem.686

Becke AD (1993) Density-functional thermochemistry. III. The role of exact exchange. J Chem Phys 98:5648–5652. https://doi.org/10.1063/1.464913

Benosmane S, Bendjelloul M, Elandaloussi EH, Touhami M, de Ménorval L-C (2021) Experimental and modeling study on adsorption of emerging contaminants onto hyper-crosslinked cellulose. Chem Pap 75:4021–4034. https://doi.org/10.1007/s11696-021-01637-4

Blöchl PE (1994) Projector augmented-wave method. Phys Rev B 50:17953–17979. https://doi.org/10.1103/PhysRevB.50.17953

Boehm HP (1966) Chemical identification of surface groups. In: Eley DD, Pines H, Weisz PB (eds) Advances in catalysis. Academic Press, Cambridge, pp 179–274

Boehm HP, Diehl E, Heck W, Sappok R (1964) Surface oxides of carbon. Angew Chem Int Ed 3:669–677. https://doi.org/10.1002/anie.196406691

Cazetta AL, Vargas AMM, Nogami EM, Kunita MH, Guilherme MR, Martins AC, Silva TL, Moraes JCG, Almeida VC (2011) NaOH-activated carbon of high surface area produced from coconut shell: Kinetics and equilibrium studies from the methylene blue adsorption. Chem Eng J 174:117–125. https://doi.org/10.1016/j.cej.2011.08.058

Chen W-f, Pan L, Chen L-f, Wang Q, Yan C-c (2014) Dechlorination of hexachlorobenzene by nano zero-valent iron/activated carbon composite: iron loading, kinetics and pathway. RSC Adv 4:46689. https://doi.org/10.1039/C4RA06760F

Crum JR (2006) Corrosion by hydrogen chloride and hydrochloric acid. In: Cramer SD, Covino BS (eds) Corrosion: environments and industries. ASM Intern, Ohio, pp 682–689

Donnet JB (1968) The chemical reactivity of carbons. Carbon 6:161–176. https://doi.org/10.1016/0008-6223(68)90300-X

Faramawy S, Zaki T, Sakr AAE (2016) Natural gas origin, composition, and processing: a review. J Nat Gas Sci Eng 34:34–54. https://doi.org/10.1016/j.jngse.2016.06.030

Georgiadis A, Charisiou N, Goula M (2020) Removal of hydrogen sulfide from various industrial gases: a review of the most promising adsorbing materials. Catalysts 10:521–556. https://doi.org/10.3390/catal10050521

GmbH UoKaFK (2010) TURBOMOLE V6.2, a Development of university of Karlsruhe and Forschungszentrum Karlsruhe GmbH, 1989–2007, TURBOMOLE GmbH, since 2007; available from http://www.turbomole.com.

Grimme S, Ehrlich S, Goerigk L (2011) Effect of the damping function in dispersion corrected density functional theory. J Comput Chem 32:1456–1465. https://doi.org/10.1002/jcc.21759

Henkelman G, Arnaldsson A, Jónsson H (2006) A fast and robust algorithm for Bader decomposition of charge density. Comput Mater Sci 36:354–360. https://doi.org/10.1016/j.commatsci.2005.04.010

Hu S, Hsieh Y-L (2017) Lignin derived activated carbon particulates as an electric supercapacitor: carbonization and activation on porous

structures and microstructures. RSC Adv 7:30459–30468. https://doi.org/10.1039/C7RA00103G
Iannarelli R, Rossi MJ (2014) H_2O and HCl trace gas kinetics on crystalline HCl hydrates and amorphous HCl/H_2O in the range 170 to 205 K: the HCl/H_2O phase diagram revisited. Atmos Chem Phys 14:5183–5204. https://doi.org/10.5194/acp-14-5183-2014
Kim K-J, Kang C-S, You Y-J, Chung M-C, Jeong SW, Jeong W-J, Woo M-W, Ahn H-G (2006) Adsorption–desorption characteristics of modified activated carbons for volatile organic compounds. Stud Surf Sci Catal 159:457–460. https://doi.org/10.1016/s0167-2991(06)81632-0
Kohn W, Sham LJ (1965) Self-consistent equations including exchange and correlation effects. Phys Rev 140:A1133–A1138. https://doi.org/10.1103/PhysRev.140.A1133
Kresse G, Furthmuller J (1996) Efficient iterative schemes for ab initio total-energy calculations using a plane-wave basis set. Phys Rev B Condens Matter 54:11169–11186. https://doi.org/10.1103/physrevb.54.11169
Kresse G, Furthmüller J (1996) Efficiency of ab-initio total energy calculations for metals and semiconductors using a plane-wave basis set. Comput Mater Sci 6:15–50. https://doi.org/10.1016/0927-0256(96)00008-0
Kresse G, Hafner J (1993) Ab initio molecular dynamics for liquid metals. Phys Rev B Condens Matter 47:558–561. https://doi.org/10.1103/physrevb.47.558
Kresse G, Joubert D (1999) From ultrasoft pseudopotentials to the projector augmented-wave method. Phys Rev B Condens Matter 59:1758–1775. https://doi.org/10.1103/PhysRevB.59.1758
Leenaerts O, Partoens B, Peeters FM (2008) Adsorption of H_2O, NH_3, CO, NO_2, and NO on graphene: a first-principles study. Phys Rev B 77:125416–125421. https://doi.org/10.1103/PhysRevB.77.125416
Lee S-W, Daud WMAW, Lee M-G (2010) Adsorption characteristics of methyl mercaptan, dimethyl disulfide, and trimethylamine on coconut-based activated carbons modified with acid and base. J Ind Eng Chem 16:973–977. https://doi.org/10.1016/j.jiec.2010.04.002
Liu L, Luo X-B, Ding L, Luo S-L (2019) Application of nanotechnology in the removal of heavy metal from water. In: Luo X, Deng F (eds) Nanomaterials for the removal of pollutants and resource reutilization. Elsevier, Amsterdam, pp 83–147
Ludlow DK (2006) Activated carbon adsorption by roop chand bansal and meenakshi Goyal (Panjab University, Chandigarh, India). CRC Press (an imprint of Taylor and Francis Group): Boca Raton, FL. 2005. Xxii + 498 pp. J Am Chem Soc 128:10630–10634. https://doi.org/10.1021/ja059874h
Marsh H, Rodríguez-Reinoso F (2006) Characterization of activated carbon. In: Marsh H, Rodríguez-Reinoso F (eds) Activated carbon. Elsevier, Amsterdam, pp 143–242
Menezes MG, Ullah S (2021) Unveiling the multilevel structure of midgap states in Sb-doped MoX_2 (X=S, Se, Te) monolayers. Phys Rev B 104:125438–125451. https://doi.org/10.1103/PhysRevB.104.125438
Mouazer R, Scheffer R (2017). Process to separate phosgene and hydrogen chloride from a fluid stream comprising phosgene and hydrogen chloride. Patent U 9533885 May 29, 2014
Osio-Norgaard J, Srubar WV (2019) Zeolite adsorption of Chloride from a Synthetic Alkali-activated cement pore solution. Materials 12:1–7. https://doi.org/10.3390/ma12122019
Perdew JP, Burke K, Ernzerhof M (1996) Generalized gradient approximation made simple. Phys Rev Lett 77:3865. https://doi.org/10.1103/PhysRevLett.77.3865
Protilla VI (1976) The nature of hydrogen bonds and water in legrandite by IR spectroscopy. Am Mineral 61:95–99
Ran J, Hao X, Li K, Wang C, Song X, Sun X, Ning P (2020) First-principles studies of HF and HCl adsorption over graphene. J Mol Model 26:1–8. https://doi.org/10.1007/s00894-020-04526-x
Sanville E, Kenny SD, Smith R, Henkelman G (2007) Improved grid-based algorithm for Bader charge allocation. J Comput Chem 28:899–908. https://doi.org/10.1002/jcc.20575
Schäfer A, Huber C, Ahlrichs R (1994) Fully optimized contracted gaussian basis sets of triple zeta valence quality for atoms Li to Kr. Chem Phys 100:5829–5835. https://doi.org/10.1063/1.467146
Shannon RD (1976) Revised effective ionic radii and systematic studies of interatomic distances in halides and chalcogenides. Acta Crystallogr A 32:751–767. https://doi.org/10.1107/S0567739476001551
Soni R, Bhardwaj S, Shukla DP (2020) Various water-treatment technologies for inorganic contaminants: current status and future aspects. In: Devi P, Singh P, Kansal SK (eds) Inorganic pollutants in water. Elsevier, Netherlands, pp 273–295
Supong A, Bhomick PC, Sinha UB, Sinha D (2019) A combined experimental and theoretical investigation of the adsorption of 4-Nitrophenol on activated biocarbon using DFT method. Korean J Chem Eng 36:2023–2034. https://doi.org/10.1007/s11814-019-0382-z
Swenson H, Stadie NP (2019) Langmuir's theory of adsorption: a centennial review. Langmuir 35:5409–5426. https://doi.org/10.1021/acs.langmuir.9b00154
Tangsathitkulchai C, Naksusuk S, Wongkoblap A, Phadungbut P, Borisut P (2021) Equilibrium and kinetics of CO_2 adsorption by coconut shell activated carbon impregnated with sodium hydroxide. Processes 9:201. https://doi.org/10.3390/pr9020201
Tolentino CMC, de Luna MDG, Futalan CM, Choi AES, Manegdeg FG, Grisdanurak N (2020) Influence of hydrocarbons on hydrogen chloride removal from refinery off-gas by zeolite NaY derived from rice husks. Sci Total Environ 728:138782–138791. https://doi.org/10.1016/j.scitotenv.2020.138782
Wang S, Nam H, Gebreegziabher TB, Nam H (2020) Adsorption of acetic acid and hydrogen sulfide using NaOH impregnated activated carbon for indoor air purification. Eng Rep 2:12083–12104. https://doi.org/10.1002/eng2.12083
Wang H, Liu G, Boon YZ, Veksha A, Giannis A, Lim TT, Lisak G (2021) Dual-functional witherite in improving chemical looping performance of iron ore and simultaneous adsorption of HCl in syngas at high temperature. Chem Eng J 413:127538–127548. https://doi.org/10.1016/j.cej.2020.127538
Weinlaender C, Neubauer R, Hauth M, Hochenauer C (2018) Adsorptive hydrogen chloride and combined hydrogen chloride–hydrogen sulphide removal from biogas for solid oxide fuel cell application. Adsorpt Sci Technol 36:1215–1232. https://doi.org/10.1177/0263617418772660
Wu F-C, Tseng R-L (2008) High adsorption capacity NaOH-activated carbon for dye removal from aqueous solution. J Hazard Mater 152:1256–1267. https://doi.org/10.1016/j.jhazmat.2007.07.109
Wu W, Wu Y, Wang T, Wang D, Gu Q, Jin B (2020) HCl removal using calcined Ca–Mg–Al layered double hydroxide in the presence of CO_2 at medium–high temperature. Catalysts 10:22–34. https://doi.org/10.3390/catal10010022
Yang Q, Wang C, Zhao Z, Wei W, Ma J, Qin G (2021) Structural and thermodynamic factors in the adsorption process of anthocyanins from eggplant peel onto a carbon adsorbent. Chem Pap 75:5687–5694. https://doi.org/10.1007/s11696-021-01748-y
You Y, Deng J, Tan X, Gorjizadeh N, Yoshimura M, Smith SC, Sahajwalla V, Joshi RK (2017) On the mechanism of gas adsorption for pristine, defective and functionalized graphene. Phys Chem Chem Phys 19:6051–6056. https://doi.org/10.1039/C6CP07654H
Yue Z, Economy J, Bordson G (2006) Preparation and characterization of NaOH-activated carbons from phenolic resin. J Mater Chem 16:1456–1461. https://doi.org/10.1039/B513267C

Yu M, Trinkle DR (2011) Accurate and efficient algorithm for Bader charge integration. Chem Phys 134:064111–064118. https://doi.org/10.1063/1.3553716

Zhang X, Li Z, Zhao J, Cui Y, Tan B, Wang J, Zhang C, He G (2017) Mechanism of Ce promoting SO_2 resistance of MnO_x/γ-Al_2O_3: an experimental and DFT study. Korean J Chem Eng 34:2065–2071. https://doi.org/10.1007/s11814-017-0092-3